Metabolic potential and survival strategies of microbial communities across extreme temperature gradients on Deception Island volcano, Antarctica

Amanda Gonçalves Bendia[1*], Leandro Nascimento Lemos[2], Lucas William Mendes[2], Camila Negrão Signori[1], Brendan J. M. Bohannan[3], Vivian Helena Pellizari[1]

[1]Departamento de Oceanografia Biológica, Instituto Oceanográfico, Universidade de São Paulo (USP). Praça do Oceanográfico, 191. CEP: 05508-900 São Paulo, SP, Brazil.

[2]Laboratório de Biologia Celular e Molecular, Centro de Energia Nuclear na Agricultura, Universidade de São Paulo. Avenida Centenário 303, CEP 13416-00 Piracicaba, SP, Brazil.

[3]Department of Biology, Institute of Ecology and Evolution, University of Oregon, Eugene, OR, United States

*Corresponding author:

Amanda Gonçalves Bendia

Address: Departamento de Oceanografia Biológica, Instituto Oceanográfico, Universidade de São Paulo, São Paulo, Brazil. Praça do Oceanográfico, 191. CEP: 05508-900 São Paulo, SP, Brazil.

Email: amandagb@usp.br

Phone number: +55 (11) 3091-6557

Running Title: Community survival strategies on Deception Island

Abstract

Active volcanoes in Antarctica, in contrast to the rest of the icy landscape, have remarkable temperature and geochemical gradients that could select for a wide variety of microbial adaptive mechanisms and metabolic pathways. Deception Island is a stratovolcano flooded by the sea, resulting in contrasting ecosystems such as permanent glaciers (<0 ^{o}C) and active fumaroles (up to 100 ^{o}C). Steep gradients in temperature, salinity and geochemistry over very short distances have been reported for Deception Island, and have been shown to effect microbial community structure and diversity. However, little is known regarding how these gradients affect ecosystem functioning, for example due to inhibition of key metabolic enzymes or pathways. In this study, we used shotgun metagenomics and metagenome-assembled genomes to explore how microbial functional diversity is shaped by extreme geochemical, salinity and temperature gradients in fumarole and glacier sediments. We observed that microbial communities from a 98 ^{o}C fumarole harbor specific hyperthermophilic molecular strategies, as well as reductive and autotrophic pathways, while those from <80 ^{o}C fumaroles possess more diverse metabolic and survival strategies capable of responding to fluctuating redox and temperature conditions. In contrast, glacier communities showed less diverse metabolic potentials, comprising mainly heterotrophic and carbon pathways. Through the reconstruction of genomes, we were able to clarify putative novel lifestyles of underrepresented taxonomic groups, especially those related to Nanoarchaeota and thermophilic ammonia-oxidizing archaeal lineages. Our results enhance understanding of the metabolic and survival capabilities of different extremophilic lineages of Bacteria and Archaea.

Key words: Deception Island, Antarctica, Microbial ecology, Microbial processes, Metagenome-assembled genomes, Extremophiles

Introduction

The study of life in extreme environments has long fascinated biologists. Understanding how life persists at environmental extremes provides insight into how living systems function, as well as providing a unique window into the evolutionary history of life itself (Merino et al., 2019). The Deception Island volcano contains a unique combination of extreme temperatures and geochemical energy sources that together have the potential for selecting a wide variety of microbial adaptive mechanisms and metabolic pathways. Deception Island is located in the South Shetland Islands at the spreading center of the Bransfield Strait marginal basin, which harbors contrasting ecosystems of permanent glaciers and active fumaroles with continuous emissions of gases, mostly carbon dioxide and hydrogen sulfide (Somoza et al., 2004). This combination of glaciers and fumaroles is produced by the interaction between the cryosphere and water mass contact with hot ascending magmas (Geyer et al., 2019). Unlike Antarctic continental volcanoes, Deception Island fumaroles reach up to 100 ^{o}C and have direct marine influence, creating a remarkable combination of thermal, geochemical and salinity gradients (Bartolini et al., 2014; Herbold et al., 2014; Muñoz-Martín et al., 2005).

While early research carried out on Deception focused primarily on obtaining bacterial isolates from hot or cold ecosystems (e.g. Carrión et al., 2011; Llarch et al., 1997; Stanley et al., 1967), a more recent study was able to recover both psychrophilic and thermophilic isolates among the steep temperature gradients (Bendia et al., 2018a). Previous molecular studies described microbial diversity on Deception fumaroles using DGGE (Amenábar et al., 2013; Muñoz et al., 2011) and shotgun metagenomics to characterize the resistome profiles in cold sediments from Whalers Bay

(Centurion et al., 2019). These previous studies were limited with respect to sampling depth and extent since only fumaroles or cold sediments were analyzed.

Two previous studies have focused on understanding the effect of Deception temperature gradients on microbial communities. The first, performed by our group, focused on determining taxonomic diversity through 16S rRNA gene sequencing (Bendia et al., 2018b), and a second study applied the Life Detector Chip (LDChip) to describe general functions of communities from Cerro Caliente (Lezcano et al., 2019). Our previous study showed that the steep gradients on Deception were able to select a unique combination of taxonomic groups found in deep and shallow hydrothermal vents (including hyperthermophilic Archaea, such as *Pyrodictium spp.*), geothermal systems and those typical from polar ecosystems (Bendia et al., 2018b). Also we reported that the bacterial community structure on Deception Island is strongly niche driven by a variety of environmental parameters (temperature, pH, salinity and volcanic geochemicals, such as sulfate), while archaeal diversity is mainly shaped by temperature (Bendia et al., 2018b). These previous studies, however, did not address the linkages between microbial structure and their adaptive and metabolic strategies over the particular environmental gradients found on Deception Island.

Although several studies have demonstrated that temperature is a primary driver of microbial taxonomic diversity in different geothermal and hydrothermal ecosystems (e.g. Antranikian et al., 2017; Price and Giovannelli, 2017; Sharp et al., 2014; Ward et al., 2017), it is still unclear to what extent temperature affects the functional processes of a microbial community, such as their adaptive mechanisms and metabolic pathways. The majority of these previous studies have focused on nonpolar thermal ecosystems, where the temperature range is narrower than in polar

volcanoes; the exception is a study of deep-sea hydrothermal vents, in which the contrasting temperatures are created by the contact of heat with the surrounding cold seawater (with temperatures 0-4 ^{o}C). Indeed, the Deception communities from fumaroles have similar members (Bendia et al., 2018b) to those found in deep-sea hydrothermal vents (e.g. Dick, 2019; Nakagawa et al., 2006; Takai et al., 2001), which suggests that, regarding differences in pressure (and other environmental effects), the wide temperature range typical of polar volcanoes and deep-sea hydrothermal vents can act as a strong selective pressure that favors (hyper)thermophilic specialists capable of thriving in high temperatures but that can also tolerate the cold surroundings.

Furthermore, there is controversy about the impact of extreme environments on microbe-microbe interactions. Although some studies have reported a decrease in the frequency of microbe-microbe interactions inferred from co-occurrence patterns (Cole et al., 2013; Merino et al., 2019; Sharp et al., 2014), others have observed the opposite trend (Lin et al., 2016; Mandakovic et al., 2018). The analysis of co-occurrence patterns is useful for examining the nature of the ecological rearrangements that take place in a microbial community facing contrasting environments (Freilich et al., 2010; Mandakovic et al., 2018).

In the current study, we assessed the microbial functional profile in fumarole and glacier sediments from two geothermal sites on the Deception Island volcano, Antarctica. For this, we performed shotgun metagenomics to unveil functional diversity and reconstructed genomes to reveal the microbes` putative lifestyles and survival capabilities, combining the genomic information with community functional profiles. Here, we hypothesize that (i) similar to what has been reported for community diversity, survival and metabolic strategies are also influenced by the combination of

123 geochemical, salinity and extreme temperature gradients; (ii) these communities follow the
124 redundancy of metabolic potential that was reported for deep-sea hydrothermal vent communities;
125 and (iii) microbe-microbe interactions decrease with increasing temperature. This study adds
126 important information regarding the ecological processes of microbial communities inhabiting a
127 steep gradient of temperature, and addresses central questions regarding the functional adaptability
128 of extremophiles in polar regions.
129
130
131 **Materials and methods**
132 **Study site and sampling strategy**
133 Deception Island (62°58′ S, 60°39′ W) is a complex stratovolcano located in the South Shetland
134 Islands, Bransfield Strait, near the Antarctic Peninsula. A past eruption occurring approximately
135 10,000 years ago collapsed the central part of the island giving rise to a flooded caldera called Port
136 Foster Bay, 9 km in diameter (Baker et al., 1975). Fumaroles are found mainly at Fumarole Bay
137 (FB), Whalers Bay (WB), and Pendulum Cove (Fermani et al., 2007; Geyer et al., 2019), and they
138 are distributed mostly in submerged and partially submerged regions (intertidal zones), with
139 temperatures varying from 40-60°C in WB and 80-100°C in FB (Rey et al., 1995; Somoza et al.,
140 2004). Carbon dioxide and hydrogen sulfide gases are emitted by fumaroles and are oxidized to
141 products such as sulfite and sulfate (Somoza et al., 2004; Zhang and Millero, 1993).
142
143 Sampling was performed during the XXXII Brazilian Antarctic Expedition (December 2013 to
144 January 2014), with logistical support from the polar vessel NPo. Almirante Maximiano. We
145 collected surface sediment samples (*ca.* 5 cm) in fumaroles and glaciers at geothermally active

146 sites in FB (62°58'02.7" S, 60°42' 36.4" W) and WB (62°58'45.1" S, 60°33'27.3" W) (Figure 1a
147 and 1b), with temperatures between 0 and 98 ^{o}C. At each site, we obtained samples from three
148 different points within the temperature gradient, and triplicates were performed for each collected
149 point, totaling 18 sediment samples. Points A and B were defined as samples collected in
150 fumaroles, while point C samples were collected from the glacier, few cm below the glacier's edge
151 (Figure 1c and 1d). The point FBA was the hottest fumarole, measuring 98 ^{o}C at the sediment
152 surface (*ca.* 20 cm). Distances between fumaroles and glaciers at each site were approximately 15
153 m, and the WB and FB transects were approximately 10 km apart. All fumaroles were in the
154 intertidal zone, except for point B from FB, which was in the subtidal zone (submerged at 50 cm
155 depth in the water column). Samples were stored at -20 °C until arrival at the University of São
156 Paulo, Brazil in April 2014.
157
158 **DNA Extraction and metagenomic sequencing**
159 To compare our results with the study performed by Bendia et al. (2018b), we used the same
160 dataset and DNA extractions as a template for the metagenomics. Due to low DNA mass even
161 after several concentration efforts, extracted DNA was subjected to multiple displacement
162 amplification (MDA) using the illustra GenomiPhi V2 DNA amplification kit (GE Healthcare,
163 Piscataway, NJ, USA), following the manufacturer's instructions. Three amplification reactions
164 per sample were pooled to obtain sufficient DNA for sequencing. DNA was then purified using
165 AMPure XP beads kit (Beckman Coulter) following the manufacturer's instructions. Library
166 constructions and shotgun metagenomic sequencing were conducted at "Laboratório Central de
167 Tecnologias de Alto Desempenho em Ciências da Vida" (LaCTAD), Universidade Estadual de

Campinas State (UNICAMP), on the Illumina Hiseq 2000 platform using 2x100 bp paired-end system.

Physical-chemical parameters

To correlate biological and environmental data, we used the physical-chemical parameters for sediments measured by Bendia et al. (2018b), which included granulometry, electrical conductivity, humidity, micronutrients (B, Cu, Fe, Mn, and Zn), organic matter, organic carbon, pH, P, Si, Na, K, Ca, Mg, Al, total nitrogen, nitrate, ammonia, and sulfate.

Taxonomic and functional inference of metagenomic reads

Reads were quality trimmed using Sickle (Joshi and Fass, 2011) with phred >30 and then uploaded to MG-RAST (Keegan et al., 2016). Functional and taxonomic profiles of reads were generated through subsystem and best hit classifications using the SEED subsystem, M5NR (non-redundant protein database) and KEGG, available in MG-RAST (Aziz et al., 2008; Kanehisa and Goto, 2000; Keegan et al., 2016; Wilke et al., 2012), with the following parameters: $1x10^{-5}$ e-value, minimum 50 bp alignment, and 60% identity. Data generated by MG-RAST were statistically analyzed using Statistical Analysis of Metagenomic Profiles (STAMP) software (Parks et al., 2014) and R software (R Development Core Team), using the packages *vegan* (Oksanen, 2007) and *ggplot* (Wickham, 2011). The *p* values were calculated using Fisher's exact two-sided test and the confidence intervals were calculated using the method of Newcombe-Wilson. Statistical comparisons were performed by grouping the samples according to environmental temperatures: glaciers, fumaroles up to 80 ^{o}C and fumarole at 98 ^{o}C. Principal component analysis (PCA) ordination was performed by using level 3 functions of SEED subsystems and then visualized in

STAMP software. Values were normalized to relative abundance for comparison of taxonomic composition across samples. In addition, Spearman correlations were performed to determine relationships between taxonomic and functional profiles and the environmental parameters. Genetic data are available in MG-RAST under the project ID mgp15628. MG-RAST IDs for each sample are described in Supplementary Table 2.

To investigate the complexity of community interactions at each sampling site, we used co-occurrence network analysis. For this, non-random co-occurrence analyses were performed using the Python module 'SparCC' (Friedman and Alm, 2012). A table of frequency of hits affiliated to the genus level was used for analysis. For each network, we considered only strong (SparCC > 0.9 or < -0.9) and highly significant ($p < 0.01$) correlations between microbial taxa. The nodes in the reconstructed network represent taxa at the genus level, whereas the edges represent significantly positive or negative correlation between nodes. The analysis of network complexity was based on a set of measures, such as the number of nodes and edges, modularity, the number of communities, average node connectivity, average path length, diameter, and cumulative degree distribution (Newman, 2003). Network visualization and property measurements were calculated with the software Gephi (Bastian et al., 2009).

Metagenomic assembly and genome reconstruction

We used two different strategies for metagenomic assembly and genomic binning of the eighteen metagenomic datasets from Deception Island volcano. First, reads were assembled using IDBA-ud (Peng et al., 2012) (-mink 50, -maxk 92, -tep 4, -min_contig 1000) and then genomic binning was performed through MaxBin 2.0 (Wu et al., 2016). Contigs were annotated using the Integrated

Microbial Genomes & Microbiomes (IMG/M) system (Markowitz et al., 2009) and archived on the JGI/IMG server under Project ID Gs0141992. IMG accession numbers for each sample are described in Supplementary Table 2.

Furthermore, reads were co-assembled using MEGAHIT v. 1.0.2. (Li et al., 2015), discarding contigs smaller than 1000 bp. Then contigs were binned using anvi'o v. 5 following the workflow described by Eren et al. (2015). Reads for each metagenome were mapped to the co-assembly using bowtie2 with default parameters (Langmead and Salzberg, 2012). A contig database was generated using the 'anvi-gen-contigs-database'. Prodigal (Hyatt et al., 2010) was used to predict open reading frames (ORFs). Single-copy bacterial and archaeal genes were identified using HMMER v. 3.1b2 (Finn et al., 2011). The program 'anvi-run-ncbi-cogs' was used to annotate genes with functions by searching for them against the December 2014 release of the Clusters of Orthologous Groups (COGs) database (Galperin et al., 2015) using blastp v2.10.0+ (Altschul et al., 1990). Predicted protein sequences were functionally and taxonomically annotated against KEGG with GhostKOALA (genus_prokaryotes) (Kanehisa et al., 2016). Individual BAM files were profiled using the program 'anvi-profile' with a minimum contig length of 4 kbp. Genome binning was performed using CONCOCT (Alneberg et al., 2013) through the 'anvi-merge' program with default parameters. We used 'anvi-interactive' to visualize the merged data and identify genome bins. Bins were then manually refined using 'anvi-refine', and completeness and contamination were estimated using 'anvi-summarize'.

Bins generated by the assembly and co-assembly approaches were quality checked through CheckM v. 1.0.7 (Parks et al., 2015), which is based on the representation of lineage-specific

marker gene sets. Bins were taxonomically classified based on genome phylogeny using GTDB-Tk (Chaumeil et al., 2020).

Taxonomic and functional annotation of metagenome-assembled genomes (MAGs)

Bins were defined as a high-quality draft (>90% complete, <5% contamination), medium-quality draft (>50% complete, <10% contamination) or low-quality draft (<50% complete, <10% contamination) metagenome assembled-genome (MAG), according to genome quality standards suggested by Bowers et al. (2017). We selected 11 MAGs based on their medium or high-quality and taxonomy, preferably selecting groups related to extremophiles or associated to sulfur and nitrogen metabolisms. Annotation of all predicted ORFs in MAGs was performed using prokka v.14.5 (Seemann, 2014). Further, proteins were compared to sequences in the KEGG Database through GhostKOALA (genus_prokaryotes) (Kanehisa et al., 2016) and in the SEED Subsystem through RASTtk (Brettin et al., 2015). Phenotypes were predicted using the PICA framework (Feldbauer et al., 2015) and PhenDB (https://phendb.csb.univie.ac.at/).

Results

To investigate links between metabolic potential and genes associated with survival strategies across extreme temperature and geochemical gradients of the Deception Island volcano, we analyzed the metagenomes of a total of eighteen samples, comprising fumaroles with temperatures of 98 ^{o}C, 80 ^{o}C, 50 ^{o}C, and 10 ^{o}C, and glaciers with temperatures around 0 ^{o}C. Shotgun sequencing of community genomic DNA on 3 lanes of Illumina HiSeq2000 produced a total of 567,410,264 paired-end reads, within which 475,895,996 were filtered by quality (Q>30) for further analyses. A total of 162,755,88 reads were taxonomically annotated as Bacteria, 3,680,020 as Archaea,

2,094,916 as Eukarya and 79,111 as viruses (Supplementary Table 2). The total number of proteins predicted in reads were 296,818,692 (62.3%). Relative abundances of the detected genes were used to compare the metabolic potential and genes related to survival strategies under environmental extremes among fumaroles and glaciers samples.

De novo assemblies of the quality-filtered reads generated a total of 543,945 contigs. The prediction of ORFs resulted in 1,396,820 putative genes, 353,731 assigned within Bacteria, 12,034 within Archaea, and 1,557 and 1,534 within Eukarya and viruses, respectively. We used different databases for assembly annotation through JGI/IMG that resulted in 487 putative 16S rRNA genes, 842,798 genes based on the COG database and 304,173 genes based on KEGG (Supplementary Table 2).

Taxonomic profile of microbial communities on the Deception Island volcano

Through the annotation of reads, we observed that the taxonomic composition in the 98 ^{o}C fumarole was distinct in comparison with other fumaroles and glaciers. Archaea were dominant in samples from the 98 ^{o}C fumarole (relative abundance between 31.5 and 87.3%), with the most abundant archaeal phyla classified as Crenarchaeota (23.8-79.3%), followed by Euryarchaeota (2.5-7.5%) and Korarchaeota (0.1-0.4%). Firmicutes (3.1-22.4%), Bacteroidetes (0.6-15.3%), Aquificae (0.3-4.6%), and Thermotogae (0.3-1.0%) were also detected in minor proportions in the 98 ^{o}C fumarole. Looking at the class level, Thermoprotei, Thermococci, Methanococci, Archaeoglobi, Methanobacteria, Methanopyri, and Methanomicrobia represented the most abundant archaeal classes (>0.1%) in the 98 ^{o}C site, and Bacilli, Gammaproteobacteria,

283 Betaproteobacteria, Fusobacteria, Flavobacteria, Aquificae (order Aquificales) and Thermotogae
284 (order Thermotogales) were the dominant classes within Bacteria (Figure 2a).
285
286 Archaea were less dominant in the other samples, with a relative abundance of 0.7-2% in fumaroles
287 <80 ºC and 0.4-0.6% in glaciers. Although some dominant phyla were common between <80 ºC
288 fumaroles and glaciers (e.g. Bacteroidetes, Proteobacteria, and Firmicutes), less dominant phyla
289 were uniquely distributed according to temperature. For example, Thaumarchaeota was
290 predominantly found in <80 ºC fumaroles (0.8-1% for Whalers Bay and 0.2-0.3% in Fumarole
291 Bay). Verrucomicrobia and Acidobacteria were only detected in glaciers (1.2-3.1% and 1-1.6%,
292 respectively) (Figure 2a). The main classes affiliated within the Bacteroidetes phylum were
293 Cytophagia, Flavobacteria and Sphingobacteria, whereas Gamma- and Alphaproteobacteria were
294 the most represented classes within Proteobacteria, followed by Beta-, Delta- and Epsilonbacteria
295 (Figure 2b). Solibacteres was the abundant class within Acidobacteria, and Verrucumicrobiaea
296 within Verrucomicrobia. Thaumarchaeota assignments were not classified at the class level using
297 reads annotation in MG-RAST. The taxonomic annotation of contigs through the IMG/M system
298 showed similar patterns when compared to reads annotation (Supplementary Figure 1).
299
300 We then used co-occurrence network analysis to explore the complexity of interactions within the
301 microbial communities in each treatment (Figure 2c). For this, we calculated SparCC correlations
302 between microbial taxa at the genus level based on metagenome reads annotated in MG-RAST. In
303 general, the complexity of the community increased with the temperature. We also noted that
304 communities of Fumarole Bay were more complex than Whalers Bay. The FBA (98 ºC) site
305 showed the highest level of complexity and a modular structure, whereas the WBC (0 ºC) site had

306 the least complex network. Interestingly, the proportion of positive/negative correlations also
307 changed according to the temperature; at higher temperatures, the proportion is even, while in
308 lower temperatures there was an increase in the number of positive correlations.
309
310 **Comparative functional profile of microbial communities on Deception Island volcano**
311 Functional profiles of metagenomes were compared using a multivariate method and hypothesis
312 test, and significant variations in all functional levels were observed between the 98 ^{o}C fumarole,
313 <80 ^{o}C fumaroles and glaciers. Clear differences between these three distinct sample groups were
314 observed through both the SEED Level 1 profile (Figure 3a) and SEED functional level through
315 PCA ordination (Figure 3b). Further, a distinct pattern between samples from the highest
316 temperature was observed. The prevalent core of functions among Deception samples were
317 "clustering-based subsystems", "carbohydrates", "amino acids and derivatives", "protein
318 metabolism", "RNA metabolism", "DNA metabolism" and "cofactors, vitamins, prosthetic groups
319 and pigments". Significant differences between sample groups and functions from level 1 of
320 SEED, calculated using Fisher's exact two-sided test and the Newcombe-Wilson method, showed
321 the highest abundance of genes belonging to the categories "DNA metabolism" (p = 0.046),
322 "protein metabolism" (p = 0.049), and "phages, prophages, transposable elements and plasmids"
323 (p = 3.97e-3) in the 98 ^{o}C fumarole in comparison with other fumaroles and glaciers. The
324 categories "nitrogen metabolism" (p = 1.07e-4), "photosynthesis" (p = 5.07e-3), "sulfur
325 metabolism" (p = 0.015), and "metabolism of aromatic compounds" (p = 0.036) exhibited the
326 highest significant values in <80 ^{o}C fumaroles when compared to the 98 ^{o}C fumarole, and "motility
327 and chemotaxis" (p = 2.71e-8), "RNA metabolism" (p = 0.01), and "protein metabolism" (p =
328 0.023) when compared to glaciers. In contrast, observations for glaciers showed more genes

329 associated with "carbohydrates" and "virulence, disease and defense" categories in comparison
330 with the 98 ºC fumarole (p = 0.049 and p = 0.036, respectively) and <80 ºC fumaroles (p = 1.68e-
331 6 and p = 0.012, respectively) (Figure 3c).
332
333 **Patterns of metabolic partitioning among extreme temperatures**
334 We observed different partitioning patterns of metabolic diversity according to environmental
335 temperatures (Figure 4). The fumarole with the highest temperature (98 ºC) exhibited metabolic
336 potential significantly higher for functions associated with sulfate reduction (p < 0.001),
337 dissimilatory nitrite reduction (p < 0.001) and carbon dioxide fixation (p < 0.001) when compared
338 to other fumaroles and glaciers. Although sulfur metabolism was abundant among all
339 temperatures, different metabolic pathways related to sulfur were observed according to the
340 temperature. While sulfate reduction was prevalent in the highest temperature fumarole, a high
341 number of genes related to inorganic sulfur assimilation (p < 0.001) and sulfur oxidation (p value
342 was not significant, p < 0.1) were detected in <80 ºC fumaroles. In general, nitrogen metabolism
343 was dominant in <80 ºC fumaroles when compared to other samples, with nitrate and nitrite
344 ammonification (p < 0.02), denitrification (p < 0.01), nitrogen fixation (p < 0.05) and ammonia
345 assimilation (p < 0.001) as the prevalent metabolic nitrogen pathways. All fumaroles showed a
346 similar abundance of genes belonging to sulfur oxidation, nitrate and nitrite ammonification, and
347 dissimilatory nitrite reduction. The genetic potential for carbon fixation was much higher in the 98
348 ºC fumarole (p < 0.01), whereas photosynthesis was mainly detected in the <80 ºC fumaroles and
349 glaciers. In glaciers, the genes identified within carbon metabolism were mainly associated with
350 heterotrophy and central carbon pathways, such as the pentose phosphate pathway and glycolysis,
351 as were respiration and fermentation. The function of carbon storage regulators was significantly

352 higher in <80 °C fumaroles, in addition to the observation of other carbon-related processes, such
353 as photosynthesis, fermentation, and carbon fixation (Figure 4).
354
355 **Community survival strategies under environmental extremes**
356 To understand community survival strategies under extreme temperature and geochemical
357 gradients, we selected genes in our metagenomes that are involved with stress response, DNA
358 repair, protein biosynthesis, and transport and chemotaxis. Although communities from all
359 samples were equally abundant in genes related to stress response, very distinct patterns of specific
360 responses were observed accordingly environmental temperature (Figure 4). The oxidative stress
361 response was markedly higher in the fumarole at 98 °C, mainly represented by glutaredoxins,
362 glutathione (redox cycle) and rubrerythrin functions (all with $p < 0.001$ in comparison with other
363 samples). Contrastingly, osmotic stress genes were prevalent in glaciers samples, represented
364 mainly by functions such as osmoregulation ($p < 0.001$), osmoprotectant (*yehX*) ($p = 0.01$),
365 aquaporin Z ($p = 0.05$) and synthesis of osmoregulated periplasmatic glucans ($p < 0.001$). The
366 abundance of genes related to heat and cold responses (thermal response) was distinctly distributed
367 among fumaroles and glaciers. General function of heat-shock proteins (including *hsp70*/*dnaK*)
368 were prevalent in glaciers and <80 °C fumaroles ($p < 0.001$), whereas specific archaeal thermal
369 responses dominated the 98 °C fumarole, such as thermosome chaperonin ($p < 0.001$, 0.7% of total
370 relative abundance), as were bacterial and archaeal heat-shocks *groEL*/*groES* ($p < 0.001$). The
371 relative abundance of cold shock *cspA* was higher in <80 °C fumaroles, followed by glaciers ($p <$
372 0.001). Glaciers and <80 °C fumaroles exhibited the highest abundance of dormancy and
373 sporulation function ($p < 0.01$) and all fumaroles had a prevalence of the universal stress protein
374 family ($p < 0.01$) (Figure 4).

375

376 Differences in abundance patterns of DNA repair, protein biosynthesis, transport and chemotaxis
377 were also observed across environmental temperatures (Supplementary Figure 2). Base excision
378 repair, recombination through *recU* and reverse gyrase (all with $p < 0.01$) were the main strategies
379 of DNA positive supercoiling and repair notably found in communities of the highest temperature
380 fumarole (98 ^{o}C). Strategies of DNA repair using *uvrABC* complex, recombination through *recA*
381 and photolyase were dominant in <80 ^{o}C fumaroles and glaciers (all with $p < 0.001$). Protein
382 biosynthesis genes were dominant in the highest temperature fumarole (98 ^{o}C); functions such as
383 universal GTPases ($p < 0.01$) and translation elongation factors in Archaea ($p < 0.001$) were
384 significantly higher when compared to the other samples. Chemotaxis genes were also prevalent
385 in the highest temperature fumarole (98 ^{o}C) ($p < 0.001$), as were several transport systems
386 (transport of Ni, Co, and Zn) and ABC transporters (e.g. branched-chain amino acid, oligopeptide
387 and tungstate) (all with at least $p < 0.05$). Mn transport and the ABC transporters of iron and
388 peptides were significantly higher in <80 ^{o}C fumaroles (all with at least $p < 0.05$) (Supplementary
389 Figure 2).

390

391 **Physical-chemical influence on taxonomic and functional diversity**

392 To identify key environmental drivers of community taxonomy (at phylum level) and function
393 (SEED level 1), Spearman correlations were calculated; then only significant ($p < 0.05$) and strong
394 correlations ($r > -0.6$ or 0.6) were considered. In general, the phyla that positively correlated with
395 temperature were Euryarchaeota, Crenarchaeota, Korarchaeota, Nanoarchaeota, Thermotogae, and
396 Aquificae, whereas several phyla were negatively correlated with temperature (e.g. Acidobacteria,
397 Bacteroidetes, Spirochaetes, Actinobacteria, Verrucumicrobia, Nitrospirae, Deinococcus-

Thermus, and Gemmatimonadetes, among others) (Figure 5a). The phyla that negatively correlated with ammonia were Proteobacteria, Thaumarchaeota, Euryarchaeota, and Deferribacteres; those positively correlated were Firmicutes, Acidobacteria, Cyanobacteria, and Spirochaetes, among others. All significant nitrate correlations were positive, including phyla such as Firmicutes, Nitrospirae, Thermotogae, etc. Sulfate showed significant positive correlations with Proteobacteria, Thaumarchaeota, Euryarchaeota, Deferribacteres and Crenarchaeota, and negative correlations with phyla such as Acidobacteria, Cyanobacteria, Actinobacteria, and Verrucomicrobia, among others. Other parameters exhibited positive and negative correlations with several phyla, such as organic matter, organic carbon, B, Cu (uniquely negative correlations), Fe (uniquely negative correlations), Na, K, Ca, Mg and Al (Figure 5a, Supplementary Table 3).

The functional categories (SEED level 1) which presented positive correlations with temperature were “DNA metabolism”, “nucleosides and nucleotides” and “RNA metabolism”, and those which exhibited negative correlations were “fatty acids, lipids and isoprenoids”, “iron acquisition”, “metabolism of aromatic compounds”, “phosphorus metabolism”, “photosynthesis”, “secondary metabolism”, “stress response”, and “sulfur metabolism” (Figure 5b). Ammonia was negatively correlated with functions such as “carbohydrates”, “motility and chemotaxis”, “respiration” and “RNA metabolism”, whereas positive correlations comprised functions as “amino acids and derivatives” and “cofactors, vitamins, prosthetic groups and pigments”. Nitrate also presented negative correlations with “carbohydrates”, “dormancy and sporulation” and “phages, prophages, transposable elements and plasmids”. In contrast, sulfate was positively correlated with “carbohydrates”, “DNA metabolism”, “motility and chemotaxis”, “respiration” and “RNA metabolism”. Other parameters exhibited positive and negative correlations with several functions,

421 such as organic matter, organic carbon, B, Cu, Fe, Si, Na, K, Ca, Mg and Al (Figure 5b,
422 Supplementary Table 3).
423
424 **Metabolic potential and survival strategies in MAGs**
425 In general, the anvi'o pipeline using co-assembly showed the best binning results for our eighteen
426 metagenomes, generating a total of 158 MAGs. We included in our analyses only 1 MAG produced
427 through the idba-ud assembler and MaxBin binning since this MAG belonged to a taxon
428 (Calditrichia) which was not achieved through the anvi'o pipeline (Supplementary Figure 3,
429 Supplementary Table 4). From the 159 MAGs, 12 were assigned as Archaea through GTDB-Tk
430 and GhostKoala, belonging to Nitrososphaerales (*Candidatus Nitrosocaldus* according with
431 GhostKoala taxonomy) (2), *Nitrosoarchaeum* (1), *Nitrosotenius* (1), *Nitrospumilus* (1),
432 Desulfurococcales (*Aeropyrum* according with GhostKoala taxonomy) (1), Acidilobaceae (1),
433 Pyrodictiaceae (2) and Woesearchaeia (Nanoarchaeota) (3). The bacterial MAGs were classified
434 through GTDB-Tk and GhostKoala as the following phyla: Acidobacteriota (1), Aquificota (2),
435 Bacteroidota (92), Calditrichota (5), Campylobacterota (1), Chloroflexota (3), Cyanobacteriota
436 (1), Firmicutes (1), Nitrospirota (2), Patescibacteria (4) and Proteobacteria (35) (Supplementary
437 Figure 4, Supplementary Table 4). A total of 13 MAGs were considered as high quality and 82 as
438 medium quality drafts.
439
440 The MAGs were selected for functional annotation by their quality and based on groups related to
441 extremophiles and associated to sulfur and nitrogen metabolisms. These 11 selected MAGs were
442 assigned as DI_MAG_00003 (*Sulfurimonas*), DI_MAG_00004
443 (Hydrogenothermaceae/*Persephonella*), DI_MAG_00006 (Promineofilaceae/*Candidatus*

444 *Promineofilum*), DI_MAG_00010 (Caldilineaceae/*Caldilinea*), DI_MAG_00011
445 (Thermonemataceae), DI_MAG_00019 (Chitinophagaceae), DI_MAG_00020
446 (Pyrodictiaceae/*Pyrodictium*), DI_MAG_00021 (Dojkabacteria), DI_MAG_00022
447 (Woesearchaeia/archaeon GW2011_AR20), DI_MAG_00049 (Nitrososphaerales/*Candidatus*
448 *Nitrosocaldus*) and DI_MAG_FBB2_12 (Calditrichia) (Table 1).
449
450 We identified in the high-quality DI_MAG_00004 (Hydrogenothermaceae/*Persephonella*, ~ 97%
451 completeness) genes for nitrate reduction (*narGHI* and *nirA*), denitrification (*narGHI*),
452 nitrification (*narGH*), sulfate reduction (*sat*, *cysH*, *sir*), sulfur and thiosulfate oxidation
453 (*soxAXBYZ*), and incomplete pathways for carbon fixation (Figure 6a). This MAG had several
454 genes associated with stress response, especially oxidative stress (e.g. superoxide reductase and
455 dismutase, rubrerythrin and rubredoxin) and thermal response (e.g. *groES*, *hsp20* and *hspR*), as
456 different DNA repair mechanisms, including photolyase repair (Figure 6b). In general, genes
457 involved with the nitrogen cycle were identified in almost all selected MAGs, except for MAGs
458 DI_MAG_00020, DI_MAG_00021, and DI_MAG_00022. Sulfate reduction genes were also
459 detected in different selected MAGs, except for MAGs DI_MAG_00020, DI_MAG_00021,
460 DI_MAG_00022 and DI_MAG_FBB2_12. All MAGs had incomplete pathways for carbon
461 fixation, except for DI_MAG_00004 and DI_MAG_00021 (Figure 6a).
462
463 Different cold-shock genes were detected among MAGs; DI_MAG_00006 was the one which
464 presented more *csp* genes. We did not find any *csp* genes in archaeal MAGs (DI_MAG_00020,
465 DI_MAG_00022, and DI_MAG_00049). However, we observed genes in all selected MAGs that
466 were related to different heat-shock responses, including *groEL/groES* genes in DI_MAG_00004,

DI_MAG_00020, and DI_MAG_00021. Thermosome (*thsA*) and reverse gyrase genes were identified in all the selected MAGs assigned as Archaea (DI_MAG_00020, DI_MAG_00022, and DI_MAG_00049). Although all MAGs showed the potential presence of oxidative stress response (except DI_MAG_00049), rubrerythrin and rubredoxin genes were only observed in DI_MAG_00004 and DI_MAG_00003. Different DNA repair mechanisms were identified in selected MAGs, such as several recombination genes (*rec* genes), DNA mismatch repair (*mut* genes), nucleotide excision repair (*uvr* genes), double-strand break repair (*her*A, only in archaeal-selected MAGs) and photolyase repair (only in DI_MAG_00004) (Figure 6b).

Discussion

The primary goal of our study was to unveil how communities functionally respond to the combination of environmental factors typical of polar marine volcanoes. Our results show that regardless of proximity between fumaroles and glaciers on Deception Island, the community function is strongly driven by the combination of contrasting environmental factors, as occurred similar to what we previously observed for community composition and diversity (Bendia et al., 2018b). We detected some bacterial groups present in both glacier and fumarole sediments (most notably the phyla Proteobacteria, Firmicutes, and Bacteroidetes), despite the strong gradients in temperature, geochemistry and salinity. In addition, we observed specific groups that varied according to the environmental temperature: the hyperthermophilic members belonging to Crenarchaeota/Thermoprotei, Aquificae and Thermotoga phyla in the 98 ^{o}C fumarole, Thaumarchaeota in <80 ^{o}C fumaroles, and Acidobacteria and Verrucomicrobia in glaciers. These patterns are consistent with previous work carried out on Deception Island using the same sample set for diversity analysis (16S rRNA gene sequencing) (Bendia et al., 2018b), except for the

490 Aquificae and Thermotogae phyla, which were not detected by that method. Furthermore, our
491 taxonomic patterns were also consistent with a previous report that observed similar members
492 along a temperature gradient ranging from 7.5 to 99 ºC in geothermal areas in Canada and New
493 Zealand (Sharp et al., 2014).
494
495 Surprisingly, our network analysis showed that the community interaction in the hottest fumarole
496 (98 ºC) was more complex and presented fewer positive interactions when compared to the lowest
497 temperatures, in contrast to previous studies that showed that community complexity decreases
498 with temperature increase (Cole et al., 2013; Merino et al., 2019; Sharp et al., 2014). Our results
499 suggest that hyperthermophilic temperatures on Deception probably trigger ecological interactions
500 between community members to modulate their resistance and resilience when facing strong
501 environmental stressors. Similar patterns of community interaction have been previously observed
502 in stressful conditions in the Atacama Desert (Mandakovic et al., 2018) and with increasing
503 temperature in anaerobic digestion (Lin et al., 2016), although these environmental conditions are
504 different from those found on Deception Island.
505
506 Correlation with environmental drivers varied among both taxonomic and functional groups. For
507 example, groups positively influenced by temperature, sulfate, and sodium were those mainly
508 abundant in fumaroles, while groups and functions prevalent in glaciers were positively correlated
509 with ammonia. These results indicate that the mosaic of environmental parameters shapes both
510 taxonomic and functional diversity of microbial communities. Indeed, we observed a partition of
511 metabolic diversity among the steep environmental gradients on Deception Island. Unlike previous
512 studies carried out at hydrothermal vents which pointed to metabolic functional redundancy at the

513 community level (Galambos et al., 2019; Reveillaud et al., 2016), Deception communities showed
514 metabolic heterogeneity across the sharp temperature gradient. The observation of functional
515 redundancy despite the taxonomic variation has been observed in several environments such as
516 venting fluids from the Mariana back-arc, cold subseafloor ecosystems, freshwater and gut
517 microbiomes (Louca et al., 2016; Trembath-Reichert et al., 2019; Tully et al., 2018; Turnbaugh
518 and Gordon, 2009; Várbíró et al., 2017). The metabolic heterogeneity observed in our results
519 indicates that microbial communities on Deception harbor a remarkably diverse genetic content
520 that reflects the strong selective pressures caused by a remarkable interaction between the volcanic
521 activity, the marine environment, and the cryosphere.
522
523 The functional pattern clustered the samples by temperature, rather than by geographic location,
524 and showed that microbial communities on Deception Island are grouped by 98 ^{o}C fumarole, <80
525 ^{o}C fumaroles and glaciers. The predominant metabolic potential in the hottest fumarole (98 ^{o}C)
526 was mostly associated with reductive pathways, such as sulfate reduction, ammonification, and
527 dissimilatory nitrite reduction, and carbon fixation. We suggest that the hydrogen sulfide emissions
528 and hyperthermophilic conditions of this fumarole (98 ^{o}C) (Somoza et al., 2004) may decrease the
529 dissolved oxygen even in the superficial sediment layers, creating a steep redox gradient and
530 preferably selecting microorganisms with reductive and autotrophic pathways. In addition,
531 communities from the hottest fumarole (98 ^{o}C) exhibited several genes related to different adaptive
532 strategies, such as those associated with oxidative stress, specific archaeal heat-shock responses,
533 base excision repair, recombination (*recU*), reverse gyrase, protein biosynthesis, chemotaxis, and
534 ABC transporters. This reflects its primaries stress factors, including the fumarolic production of
535 hydrogen sulfide, which has a strong reductive power capable of causing oxidative stress, and

536 hyperthermophilic temperature that induces disturbance to metabolic processes and cell-
537 component denaturation (Hedlund et al., 2015; Merino et al., 2019). Enrichment in genes involved
538 with chemotaxis was also observed in metagenomes from hydrothermal vents at Juan de Fuca
539 Ridge (Xie et al., 2011), but different DNA repair mechanisms were found when compared to
540 Deception metagenomes. Different types of ABC transporters were also detected in Ilheya
541 hydrothermal fields (Wang and Sun, 2017); reverse gyrase and thermosome mechanisms have
542 often been described in several groups of hyper(thermophilic) Archaea (Forterre et al., 2000;
543 Lemmens et al., 2018; Lulchev and Klostermeier, 2014).
544
545 In contrast, <80 ^{o}C fumaroles were dominated by genes involved with different energetic and
546 chemolithotrophic pathways: sulfur oxidation, ammonification, denitrification, nitrogen fixation,
547 and dissimilatory nitrite reduction. This suggests a trend for both reductive and oxidative
548 pathways, as well as metabolic versatility and complex biogeochemical processes at the local
549 community level. Although genes related to sulfur and nitrogen pathways were detected in
550 glaciers, the majority of potential pathways for glacier communities were related to carbon
551 metabolism and heterotrophy. This lowest metabolic diversity can be explained by the decrease of
552 marine and volcanic geochemicals (e.g. sulfate) towards glaciers (Supplementary Table 1), making
553 these substrates unavailable for exploiting different energy sources, as occurs in fumaroles. The
554 <80 ^{o}C fumaroles and glacier communities harbored mechanisms for both heat and cold-shock
555 genes, dormancy and sporulation functions, and DNA repair mechanisms through *uvrABC*
556 complex, *recA*, and photolyase. Diverse survival strategies in <80 ^{o}C fumaroles and glaciers might
557 be explained by community exposure to fluctuating temperatures and redox conditions that are
558 more variable when compared to the stability of hottest fumarole, which maintains the

559 hyperthermophilic temperatures and hydrogen sulfide emissions for long periods. Further, glacier
560 communities exhibited more genes associated with osmotic stress, which reflects the low liquid
561 water availability due to the predominant freezing conditions of the Antarctic ecosystems (Wei et
562 al., 2016).
563
564 Although several studies have shown a quantitative decrease in microbial diversity as temperature
565 increases in both geothermal and hydrothermal ecosystems (Cole et al., 2013; Sharp et al., 2014),
566 little is known about how temperature affects ecosystem functioning due to inhibition of key
567 metabolic enzymes or pathways (Hedlund et al., 2015). Despite the limitation of metagenomics in
568 revealing the truly active microbial metabolic pathways, our results increase understanding of the
569 potential temperature limits on different microbial metabolism at the community level and
570 encourage more studies to elucidate the direct effect of temperature extremes on specific
571 biogeochemical processes in Antarctic volcanic ecosystems.
572
573 The 159 MAGs recovered from the Deception Island volcano comprised a broad phylogenetic
574 range of archaeal and bacterial phyla. The 11 MAGs selected for annotation included
575 hyperthermophilic and thermophilic lineages, as well as lineages containing homologs of different
576 predicted sulfur and nitrogen pathways, and archaeal groups underrepresented in genome data,
577 such as *Ca. Nitrosocaldus* and Nanoarchaeota/Woesearchaeia. Since *Ca. Nitrosocaldus* was
578 previously reported only in terrestrial geothermal environments (Abby et al., 2018; Daebeler et al.,
579 2018; Torre et al., 2008), their presence on Deception fumaroles represents a novel outcome for
580 the ecological distribution of thermophilic ammonia-oxidizing Archaea and encourages further
581 investigation to better understand their role in marine volcanic ecosystems. Furthermore, the

582 majority of our selected MAGs are equipped with gene-encoding proteins that protect cells against
583 several stressful conditions, including cold and heat-shock, carbon starvation, oxidative and
584 periplasmic stress, and DNA damage, likely enabling survival and adaptation of these
585 microorganisms to a broad combination of extreme parameters. One of our MAGs was closely
586 related to archaeon GW2011_AR20, which is an uncultivated and underrepresented
587 Nanoarchaeota/Woesearchaeia member described previously in aquifer samples and appears to
588 have a symbiotic or pathogenic lifestyle due to the small genome size and lack of some
589 biosynthesis pathways (Castelle et al., 2015). The genome analysis of our Woesearchaeia MAG
590 (archaeon GW2011_AR20, DI_MAG_00022) suggests a novel putative thermophilic lifestyle or
591 at least a potential heat tolerance for this lineage due to the (i) lack of cold-shock genes, (these
592 genes are mostly absent in the genomes of thermophilic archaea, while usually present in
593 psychrophilic/mesophilic archaeal members (Cavicchioli, 2006; Giaquinto et al., 2007), and (ii)
594 the presence of reverse gyrase, thermosome and other heat-shock genes (e.g. *groES*) that are
595 essentially related to (hyper)thermophiles and heat response. Although these heat-shock genes
596 were also detected in some mesophilic archaeal lineages within Halobacteria, Thaumarchaeota,
597 and *Methanosarcina* spp. (Lemmens et al., 2018), reverse gyrase is the only protein found
598 ubiquitously in hyperthermophilic organisms, but absent in mesophiles (Catchpole and Forterre,
599 2019), pointing to this Woesearchaeia member as a likely thermophile or hyperthermophile.
600

601 **Conclusion**

602 By combining the annotation of reads and contigs together with genome reconstruction from
603 metagenomic data, we provide the first genetic and genomic evidence that microorganisms
604 inhabiting the Deception Island volcano possess a variety of adaptive strategies and metabolic

605 processes that are shaped by steep environmental gradients. We observed that hyperthermophilic
606 temperatures (98 ^{o}C) preferably select microorganisms with reductive and autotrophic pathways,
607 while communities from fumaroles <80 ^{o}C show a high metabolic versatility with both reductive
608 and oxidative pathways, and glaciers harbor communities with metabolic processes especially
609 related to carbon metabolism and heterotrophy. Survival strategies of microorganisms from the
610 hottest fumarole are very specialized in responding to the hyperthermophilic temperatures and
611 oxidative stress, while <80 ^{o}C fumaroles and glacier communities possesses a variety of strategies
612 that are capable of responding to fluctuating redox and temperature conditions. We found more
613 complex and negative interactions among the communities from the hottest fumarole (98 ^{o}C),
614 which indicate that the strong environmental stressors probably trigger competitive associations
615 among community members. Furthermore, through the reconstruction of MAGs, we were able to
616 clarify a putative novel thermophilic lifestyle for a Woesearchaeia member and a marine lifestyle
617 for a *Ca. Nitrosocaldus* lineage. Our work represents, as far as we know, the first study to reveal
618 through shotgun metagenomics the response of microbial functional diversity to the extreme
619 temperature gradient (0 to 98^{o}C) of an Antarctic volcano. Furthermore, our study was one of the
620 first to recover MAGs from these ecosystems and it provides new insights regarding the metabolic
621 and survival capabilities of different extremophiles inhabiting the Antarctic volcanoes.
622
623
624
625
626
627

Author Contributions

AB collected the samples, conceived and designed the experiments, performed the experiments, analyzed the data, performed bioinformatic analysis, wrote the paper, and prepared figures and tables. LL contributed to discussion of metagenome-assembled genome analysis, discussed the data, wrote the paper, and reviewed drafts of the paper. LM performed network analysis, wrote the paper, and reviewed drafts of the paper. CS discussed the data, wrote the paper, and reviewed drafts of the paper. BB discussed the data, wrote and reviewed drafts of the paper. VP conceived and designed the experiments, contributed reagents, materials, and analysis tools, and wrote and reviewed drafts of the paper.

Funding

This study was part of the projects Microsfera (CNPq 407816/2013-5) and INCT-Criosfera (CNPq 028306/2009) and supported by the Brazilian National Council of Technological and Scientific Development (CNPq) and the Brazilian Antarctic Program (ProAntar). The São Paulo Research Foundation – FAPESP supported ABs Doctoral fellowship (2012/23241-0).

Conflict of Interest Statement

The authors declare that the research was conducted in the absence of any commercial or financial relationships that could be construed as a potential conflict of interest.

Acknowledgments

We thank the captain and the crew of the research polar vessel Almirante Maximiano, Dr. Luiz Henrique Rosa, Dr. Wânia Duleba, and Dr. Antônio Carlos Rocha Campos for their support in sampling. We are very thankful to LECOM's research team and Rosa C. Gamba for their scientific support.

References

Abby, S.S., Melcher, M., Kerou, M., Krupovic, M., Stieglmeier, M., Rossel, C., Pfeifer, K., Schleper, C., 2018. Candidatus Nitrosocaldus cavascurensis, an Ammonia Oxidizing, Extremely Thermophilic Archaeon with a Highly Mobile Genome. Front. Microbiol. 9. https://doi.org/10.3389/fmicb.2018.00028

Alneberg, J., Bjarnason, B.S., de Bruijn, I., Schirmer, M., Quick, J., Ijaz, U.Z., Loman, N.J., Andersson, A.F., Quince, C., 2013. CONCOCT: Clustering cONtigs on COverage and ComposiTion. ArXiv13124038 Q-Bio.

Altschul, S.F., Gish, W., Miller, W., Myers, E.W., Lipman, D.J., 1990. Basic local alignment search tool. J. Mol. Biol. 215, 403–410. https://doi.org/10.1016/S0022-2836(05)80360-2

Amenábar, M.J., Flores, P.A., Pugin, B., Boehmwald, F.A., Blamey, J.M., 2013. Archaeal diversity from hydrothermal systems of Deception Island, Antarctica. Polar Biol. 36, 373–380. https://doi.org/10.1007/s00300-012-1267-3

Antranikian, G., Suleiman, M., Schäfers, C., Adams, M.W.W., Bartolucci, S., Blamey, J.M., Birkeland, N.-K., Bonch-Osmolovskaya, E., da Costa, M.S., Cowan, D., Danson, M., Forterre, P., Kelly, R., Ishino, Y., Littlechild, J., Moracci, M., Noll, K., Oshima, T., Robb, F., Rossi, M., Santos, H., Schönheit, P., Sterner, R., Thauer, R., Thomm, M., Wiegel, J., Stetter, K.O., 2017. Diversity of bacteria and archaea from two shallow marine hydrothermal vents from Vulcano Island. Extremophiles 21, 733–742. https://doi.org/10.1007/s00792-017-0938-y

Aziz, R.K., Bartels, D., Best, A.A., DeJongh, M., Disz, T., Edwards, R.A., Formsma, K., Gerdes, S., Glass, E.M., Kubal, M., Meyer, F., Olsen, G.J., Olson, R., Osterman, A.L., Overbeek, R.A., McNeil, L.K., Paarmann, D., Paczian, T., Parrello, B., Pusch, G.D., Reich, C., Stevens, R., Vassieva, O., Vonstein, V., Wilke, A., Zagnitko, O., 2008. The RAST Server: Rapid Annotations using Subsystems Technology. BMC Genomics 9, 75. https://doi.org/10.1186/1471-2164-9-75

Baker, P.E., McReath, I., Harvey, M.R., Roobol, M.J., Davies, T.G., 1975. The geology of the South Shetland Islands: V. Volcanic evolution of Deception Island. British Antarctic Survey, Cambridge.

Bartolini, S., Geyer, A., Martí, J., Pedrazzi, D., Aguirre-Díaz, G., 2014. Volcanic hazard on Deception Island (South Shetland Islands, Antarctica). J. Volcanol. Geotherm. Res. 285, 150–168. https://doi.org/10.1016/j.jvolgeores.2014.08.009

Bastian, M., Heymann, S., Jacomy, M., 2009. Gephi: An Open Source Software for Exploring and Manipulating Networks, in: Third International AAAI Conference on Weblogs and Social Media. Presented at the Third International AAAI Conference on Weblogs and Social Media.

Bendia, A.G., Araujo, G.G., Pulschen, A.A., Contro, B., Duarte, R.T.D., Rodrigues, F., Galante, D., Pellizari, V.H., 2018a. Surviving in hot and cold: psychrophiles and thermophiles from Deception Island volcano, Antarctica. Extremophiles 22, 917–929. https://doi.org/10.1007/s00792-018-1048-1

Bendia, A.G., Signori, C.N., Franco, D.C., Duarte, R.T.D., Bohannan, B.J.M., Pellizari, V.H., 2018b. A Mosaic of Geothermal and Marine Features Shapes Microbial Community

Structure on Deception Island Volcano, Antarctica. Front. Microbiol. 9. https://doi.org/10.3389/fmicb.2018.00899

Bowers, R.M., Kyrpides, N.C., Stepanauskas, R., Harmon-Smith, M., Doud, D., Reddy, T.B.K., Schulz, F., Jarett, J., Rivers, A.R., Eloe-Fadrosh, E.A., Tringe, S.G., Ivanova, N.N., Copeland, A., Clum, A., Becraft, E.D., Malmstrom, R.R., Birren, B., Podar, M., Bork, P., Weinstock, G.M., Garrity, G.M., Dodsworth, J.A., Yooseph, S., Sutton, G., Glöckner, F.O., Gilbert, J.A., Nelson, W.C., Hallam, S.J., Jungbluth, S.P., Ettema, T.J.G., Tighe, S., Konstantinidis, K.T., Liu, W.-T., Baker, B.J., Rattei, T., Eisen, J.A., Hedlund, B., McMahon, K.D., Fierer, N., Knight, R., Finn, R., Cochrane, G., Karsch-Mizrachi, I., Tyson, G.W., Rinke, C., Lapidus, A., Meyer, F., Yilmaz, P., Parks, D.H., Eren, A.M., Schriml, L., Banfield, J.F., Hugenholtz, P., Woyke, T., 2017. Minimum information about a single amplified genome (MISAG) and a metagenome-assembled genome (MIMAG) of bacteria and archaea. Nat. Biotechnol. 35, 725–731. https://doi.org/10.1038/nbt.3893

Brettin, T., Davis, J.J., Disz, T., Edwards, R.A., Gerdes, S., Olsen, G.J., Olson, R., Overbeek, R., Parrello, B., Pusch, G.D., Shukla, M., Thomason, J.A., Stevens, R., Vonstein, V., Wattam, A.R., Xia, F., 2015. RASTtk: A modular and extensible implementation of the RAST algorithm for building custom annotation pipelines and annotating batches of genomes. Sci. Rep. 5, 8365. https://doi.org/10.1038/srep08365

Carrión, O., Miñana-Galbis, D., Montes, M.J., Mercadé, E., 2011. Pseudomonas deceptionensis sp. nov., a psychrotolerant bacterium from the Antarctic. Int. J. Syst. Evol. Microbiol. 61, 2401–2405. https://doi.org/10.1099/ijs.0.024919-0

Castelle, C.J., Wrighton, K.C., Thomas, B.C., Hug, L.A., Brown, C.T., Wilkins, M.J., Frischkorn, K.R., Tringe, S.G., Singh, A., Markillie, L.M., Taylor, R.C., Williams, K.H., Banfield, J.F., 2015. Genomic Expansion of Domain Archaea Highlights Roles for Organisms from New Phyla in Anaerobic Carbon Cycling. Curr. Biol. 25, 690–701. https://doi.org/10.1016/j.cub.2015.01.014

Catchpole, R.J., Forterre, P., 2019. The Evolution of Reverse Gyrase Suggests a Nonhyperthermophilic Last Universal Common Ancestor. Mol. Biol. Evol. 36, 2737–2747. https://doi.org/10.1093/molbev/msz180

Cavicchioli, R., 2006. Cold-adapted archaea. Nat. Rev. Microbiol. 4, 331–343. https://doi.org/10.1038/nrmicro1390

Centurion, V.B., Delforno, T.P., Lacerda-Júnior, G.V., Duarte, A.W.F., Silva, L.J., Bellini, G.B., Rosa, L.H., Oliveira, V.M., 2019. Unveiling resistome profiles in the sediments of an Antarctic volcanic island. Environ. Pollut. 255, 113240. https://doi.org/10.1016/j.envpol.2019.113240

Chaumeil, P.-A., Mussig, A.J., Hugenholtz, P., Parks, D.H., 2020. GTDB-Tk: a toolkit to classify genomes with the Genome Taxonomy Database. Bioinformatics 36, 1925–1927. https://doi.org/10.1093/bioinformatics/btz848

Cole, J.K., Peacock, J.P., Dodsworth, J.A., Williams, A.J., Thompson, D.B., Dong, H., Wu, G., Hedlund, B.P., 2013. Sediment microbial communities in Great Boiling Spring are controlled by temperature and distinct from water communities. ISME J. 7, 718–729. https://doi.org/10.1038/ismej.2012.157

Daebeler, A., Herbold, C.W., Vierheilig, J., Sedlacek, C.J., Pjevac, P., Albertsen, M., Kirkegaard, R.H., de la Torre, J.R., Daims, H., Wagner, M., 2018. Cultivation and Genomic Analysis of "Candidatus Nitrosocaldus islandicus," an Obligately Thermophilic, Ammonia-

747 Oxidizing Thaumarchaeon from a Hot Spring Biofilm in Graendalur Valley, Iceland. Front.
748 Microbiol. 9. https://doi.org/10.3389/fmicb.2018.00193
749 Dick, G.J., 2019. The microbiomes of deep-sea hydrothermal vents: distributed globally, shaped
750 locally. Nat. Rev. Microbiol. 17, 271–283. https://doi.org/10.1038/s41579-019-0160-2
751 Eren, A.M., Esen, Ö.C., Quince, C., Vineis, J.H., Morrison, H.G., Sogin, M.L., Delmont, T.O.,
752 2015. Anvi'o: an advanced analysis and visualization platform for 'omics data. PeerJ 3,
753 e1319. https://doi.org/10.7717/peerj.1319
754 Feldbauer, R., Schulz, F., Horn, M., Rattei, T., 2015. Prediction of microbial phenotypes based on
755 comparative genomics. BMC Bioinformatics 16, S1. https://doi.org/10.1186/1471-2105-
756 16-S14-S1
757 Fermani, P., Mataloni, G., Van de Vijver, B., 2007. Soil microalgal communities on an antarctic
758 active volcano (Deception Island, South Shetlands). Polar Biol. 30, 1381–1393.
759 https://doi.org/10.1007/s00300-007-0299-6
760 Finn, R.D., Clements, J., Eddy, S.R., 2011. HMMER web server: interactive sequence similarity
761 searching. Nucleic Acids Res. 39, W29–W37. https://doi.org/10.1093/nar/gkr367
762 Forterre, P., Tour, C.B. de la, Philippe, H., Duguet, M., 2000. Reverse gyrase from
763 hyperthermophiles: probable transfer of a thermoadaptation trait from Archaea to Bacteria.
764 Trends Genet. 16, 152–154. https://doi.org/10.1016/S0168-9525(00)01980-6
765 Freilich, S., Kreimer, A., Meilijson, I., Gophna, U., Sharan, R., Ruppin, E., 2010. The large-scale
766 organization of the bacterial network of ecological co-occurrence interactions. Nucleic
767 Acids Res. 38, 3857–3868. https://doi.org/10.1093/nar/gkq118
768 Friedman, J., Alm, E.J., 2012. Inferring Correlation Networks from Genomic Survey Data. PLoS
769 Comput. Biol. 8. https://doi.org/10.1371/journal.pcbi.1002687
770 Galambos, D., Anderson, R.E., Reveillaud, J., Huber, J.A., 2019. Genome-resolved metagenomics
771 and metatranscriptomics reveal niche differentiation in functionally redundant microbial
772 communities at deep-sea hydrothermal vents. Environ. Microbiol. 21, 4395–4410.
773 https://doi.org/10.1111/1462-2920.14806
774 Galperin, M.Y., Makarova, K.S., Wolf, Y.I., Koonin, E.V., 2015. Expanded microbial genome
775 coverage and improved protein family annotation in the COG database. Nucleic Acids Res.
776 43, D261–D269. https://doi.org/10.1093/nar/gku1223
777 Geyer, A., Álvarez-Valero, A.M., Gisbert, G., Aulinas, M., Hernández-Barreña, D., Lobo, A.,
778 Marti, J., 2019. Deciphering the evolution of Deception Island's magmatic system. Sci.
779 Rep. 9, 373. https://doi.org/10.1038/s41598-018-36188-4
780 Giaquinto, L., Curmi, P.M.G., Siddiqui, K.S., Poljak, A., DeLong, E., DasSarma, S., Cavicchioli,
781 R., 2007. Structure and Function of Cold Shock Proteins in Archaea. J. Bacteriol. 189,
782 5738–5748. https://doi.org/10.1128/JB.00395-07
783 Hedlund, B.P., Thomas, S.C., Dodsworth, J.A., Zhang, C.L., 2015. Life in High-Temperature
784 Environments, in: Manual of Environmental Microbiology. John Wiley & Sons, Ltd, pp.
785 4.3.4-1-4.3.4-15. https://doi.org/10.1128/9781555818821.ch4.3.4
786 Herbold, C.W., McDonald, I.R., Cary, S.C., 2014. Microbial Ecology of Geothermal Habitats in
787 Antarctica, in: Cowan, D.A. (Ed.), Antarctic Terrestrial Microbiology: Physical and
788 Biological Properties of Antarctic Soils. Springer, Berlin, Heidelberg, pp. 181–215.
789 https://doi.org/10.1007/978-3-642-45213-0_10
790 Hyatt, D., Chen, G.-L., LoCascio, P.F., Land, M.L., Larimer, F.W., Hauser, L.J., 2010. Prodigal:
791 prokaryotic gene recognition and translation initiation site identification. BMC
792 Bioinformatics 11, 119. https://doi.org/10.1186/1471-2105-11-119

Joshi, N., Fass, J., 2011. Sickle: A sliding-window, adaptive, quality-based trimming tool for FastQ files (Version 1.33) [Software].

Kanehisa, M., Goto, S., 2000. KEGG: Kyoto Encyclopedia of Genes and Genomes. Nucleic Acids Res. 28, 27–30. https://doi.org/10.1093/nar/28.1.27

Kanehisa, M., Sato, Y., Morishima, K., 2016. BlastKOALA and GhostKOALA: KEGG Tools for Functional Characterization of Genome and Metagenome Sequences. J. Mol. Biol., Computation Resources for Molecular Biology 428, 726–731. https://doi.org/10.1016/j.jmb.2015.11.006

Keegan, K.P., Glass, E.M., Meyer, F., 2016. MG-RAST, a Metagenomics Service for Analysis of Microbial Community Structure and Function, in: Martin, F., Uroz, S. (Eds.), Microbial Environmental Genomics (MEG), Methods in Molecular Biology. Springer, New York, NY, pp. 207–233. https://doi.org/10.1007/978-1-4939-3369-3_13

Langmead, B., Salzberg, S.L., 2012. Fast gapped-read alignment with Bowtie 2. Nat. Methods 9, 357–359. https://doi.org/10.1038/nmeth.1923

Lemmens, L., Baes, R., Peeters, E., 2018. Heat shock response in archaea. Emerg. Top. Life Sci. 2, 581–593. https://doi.org/10.1042/ETLS20180024

Lezcano, M.Á., Moreno-Paz, M., Carrizo, D., Prieto-Ballesteros, O., Fernández-Martínez, M.Á., Sánchez-García, L., Blanco, Y., Puente-Sánchez, F., de Diego-Castilla, G., García-Villadangos, M., Fairén, A.G., Parro, V., 2019. Biomarker Profiling of Microbial Mats in the Geothermal Band of Cerro Caliente, Deception Island (Antarctica): Life at the Edge of Heat and Cold. Astrobiology 19, 1490–1504. https://doi.org/10.1089/ast.2018.2004

Li, D., Liu, C.-M., Luo, R., Sadakane, K., Lam, T.-W., 2015. MEGAHIT: an ultra-fast single-node solution for large and complex metagenomics assembly via succinct de Bruijn graph. Bioinformatics 31, 1674–1676. https://doi.org/10.1093/bioinformatics/btv033

Lin, Q., De Vrieze, J., Li, J., Li, X., 2016. Temperature affects microbial abundance, activity and interactions in anaerobic digestion. Bioresour. Technol. 209, 228–236. https://doi.org/10.1016/j.biortech.2016.02.132

Llarch, À., Logan, N.A., Castellví, J., Prieto, M.J., Guinea, J., 1997. Isolation and Characterization of Thermophilic Bacillus spp. from Geothermal Environments on Deception Island, South Shetland Archipelago. Microb. Ecol. 34, 58–65. https://doi.org/10.1007/s002489900034

Louca, S., Parfrey, L.W., Doebeli, M., 2016. Decoupling function and taxonomy in the global ocean microbiome. Science 353, 1272–1277. https://doi.org/10.1126/science.aaf4507

Lulchev, P., Klostermeier, D., 2014. Reverse gyrase—recent advances and current mechanistic understanding of positive DNA supercoiling. Nucleic Acids Res. 42, 8200–8213. https://doi.org/10.1093/nar/gku589

Mandakovic, D., Rojas, C., Maldonado, J., Latorre, M., Travisany, D., Delage, E., Bihouée, A., Jean, G., Díaz, F.P., Fernández-Gómez, B., Cabrera, P., Gaete, A., Latorre, C., Gutiérrez, R.A., Maass, A., Cambiazo, V., Navarrete, S.A., Eveillard, D., González, M., 2018. Structure and co-occurrence patterns in microbial communities under acute environmental stress reveal ecological factors fostering resilience. Sci. Rep. 8, 5875. https://doi.org/10.1038/s41598-018-23931-0

Markowitz, V.M., Mavromatis, K., Ivanova, N.N., Chen, I.-M.A., Chu, K., Kyrpides, N.C., 2009. IMG ER: a system for microbial genome annotation expert review and curation. Bioinformatics 25, 2271–2278. https://doi.org/10.1093/bioinformatics/btp393

Merino, N., Aronson, H.S., Bojanova, D.P., Feyhl-Buska, J., Wong, M.L., Zhang, S., Giovannelli, D., 2019. Living at the Extremes: Extremophiles and the Limits of Life in a Planetary Context. Front. Microbiol. 10. https://doi.org/10.3389/fmicb.2019.00780

Muñoz, P.A., Flores, P.A., Boehmwald, F.A., Blamey, J.M., 2011. Thermophilic bacteria present in a sample from Fumarole Bay, Deception Island. Antarct. Sci. 23, 549–555. https://doi.org/10.1017/S0954102011000393

Muñoz-Martín, A., Catalán, M., Martín-Dávila, J., Carbó, A., 2005. Upper crustal structure of Deception Island area (Bransfield Strait, Antarctica) from gravity and magnetic modelling. Antarct. Sci. 17, 213–224. https://doi.org/10.1017/S0954102005002622

Nakagawa, T., Takai, K., Suzuki, Y., Hirayama, H., Konno, U., Tsunogai, U., Horikoshi, K., 2006. Geomicrobiological exploration and characterization of a novel deep-sea hydrothermal system at the TOTO caldera in the Mariana Volcanic Arc. Environ. Microbiol. 8, 37–49. https://doi.org/10.1111/j.1462-2920.2005.00884.x

Newman, M., 2003. The Structure and Function of Complex Networks. Struct. Funct. Complex Netw. 45, 167–256. https://doi.org/10.1137/S003614450342480

Oksanen, J., 2007. vegan : Community Ecology Package. R package version 1.8-5 [WWW Document]. URL /paper/vegan-%3A-Community-Ecology-Package.-R-package-1.8-5-Oksanen/ce62be133614e05a8a63c39743e42a43765a5db0 (accessed 6.3.20).

Parks, D.H., Imelfort, M., Skennerton, C.T., Hugenholtz, P., Tyson, G.W., 2015. CheckM: assessing the quality of microbial genomes recovered from isolates, single cells, and metagenomes. Genome Res. 25, 1043–1055. https://doi.org/10.1101/gr.186072.114

Parks, D.H., Tyson, G.W., Hugenholtz, P., Beiko, R.G., 2014. STAMP: statistical analysis of taxonomic and functional profiles. Bioinformatics 30, 3123–3124. https://doi.org/10.1093/bioinformatics/btu494

Peng, Y., Leung, H.C.M., Yiu, S.M., Chin, F.Y.L., 2012. IDBA-UD: a de novo assembler for single-cell and metagenomic sequencing data with highly uneven depth. Bioinformatics 28, 1420–1428. https://doi.org/10.1093/bioinformatics/bts174

Price, R.E., Giovannelli, D., 2017. A Review of the Geochemistry and Microbiology of Marine Shallow-Water Hydrothermal Vents, in: Reference Module in Earth Systems and Environmental Sciences. Elsevier. https://doi.org/10.1016/B978-0-12-409548-9.09523-3

Reveillaud, J., Reddington, E., McDermott, J., Algar, C., Meyer, J.L., Sylva, S., Seewald, J., German, C.R., Huber, J.A., 2016. Subseafloor microbial communities in hydrogen-rich vent fluids from hydrothermal systems along the Mid-Cayman Rise. Environ. Microbiol. 18, 1970–1987. https://doi.org/10.1111/1462-2920.13173

Rey, J., Somoza, L., Martínez-Frías, J., 1995. Tectonic, volcanic, and hydrothermal event sequence on Deception Island (Antarctica). Geo-Mar. Lett. 15, 1–8. https://doi.org/10.1007/BF01204491

Seemann, T., 2014. Prokka: rapid prokaryotic genome annotation. Bioinformatics 30, 2068–2069. https://doi.org/10.1093/bioinformatics/btu153

Sharp, C.E., Brady, A.L., Sharp, G.H., Grasby, S.E., Stott, M.B., Dunfield, P.F., 2014. Humboldt's spa: microbial diversity is controlled by temperature in geothermal environments. ISME J. 8, 1166–1174. https://doi.org/10.1038/ismej.2013.237

Somoza, L., Martínez-Frías, J., Smellie, J.L., Rey, J., Maestro, A., 2004. Evidence for hydrothermal venting and sediment volcanism discharged after recent short-lived volcanic eruptions at Deception Island, Bransfield Strait, Antarctica. Mar. Geol. 203, 119–140. https://doi.org/10.1016/S0025-3227(03)00285-8

Stanley, S.O., Rose, A.H., Smith, J.E., 1967. Bacteria and yeasts from lakes on Deception Island. Philos. Trans. R. Soc. Lond. B. Biol. Sci. 252, 199–207. https://doi.org/10.1098/rstb.1967.0012

Takai, K., Komatsu, T., Inagaki, F., Horikoshi, K., 2001. Distribution of Archaea in a Black Smoker Chimney Structure. Appl. Environ. Microbiol. 67, 3618–3629. https://doi.org/10.1128/AEM.67.8.3618-3629.2001

Torre, J.R.D.L., Walker, C.B., Ingalls, A.E., Könneke, M., Stahl, D.A., 2008. Cultivation of a thermophilic ammonia oxidizing archaeon synthesizing crenarchaeol. Environ. Microbiol. 10, 810–818. https://doi.org/10.1111/j.1462-2920.2007.01506.x

Trembath-Reichert, E., Butterfield, D.A., Huber, J.A., 2019. Active subseafloor microbial communities from Mariana back-arc venting fluids share metabolic strategies across different thermal niches and taxa. ISME J. 13, 2264–2279. https://doi.org/10.1038/s41396-019-0431-y

Tully, B.J., Wheat, C.G., Glazer, B.T., Huber, J.A., 2018. A dynamic microbial community with high functional redundancy inhabits the cold, oxic subseafloor aquifer. ISME J. 12, 1–16. https://doi.org/10.1038/ismej.2017.187

Turnbaugh, P.J., Gordon, J.I., 2009. The core gut microbiome, energy balance and obesity. J. Physiol. 587, 4153–4158. https://doi.org/10.1113/jphysiol.2009.174136

Várbíró, G., Görgényi, J., Tóthmérész, B., Padisák, J., Hajnal, É., Borics, G., 2017. Functional redundancy modifies species–area relationship for freshwater phytoplankton. Ecol. Evol. 7, 9905–9913. https://doi.org/10.1002/ece3.3512

Wang, H., Sun, L., 2017. Comparative metagenomics reveals insights into the deep-sea adaptation mechanism of the microorganisms in Iheya hydrothermal fields. World J. Microbiol. Biotechnol. 33, 86. https://doi.org/10.1007/s11274-017-2255-0

Ward, L., Taylor, M.W., Power, J.F., Scott, B.J., McDonald, I.R., Stott, M.B., 2017. Microbial community dynamics in Inferno Crater Lake, a thermally fluctuating geothermal spring. ISME J. 11, 1158–1167. https://doi.org/10.1038/ismej.2016.193

Wei, S.T.S., Lacap-Bugler, D.C., Lau, M.C.Y., Caruso, T., Rao, S., de los Rios, A., Archer, S.K., Chiu, J.M.Y., Higgins, C., Van Nostrand, J.D., Zhou, J., Hopkins, D.W., Pointing, S.B., 2016. Taxonomic and Functional Diversity of Soil and Hypolithic Microbial Communities in Miers Valley, McMurdo Dry Valleys, Antarctica. Front. Microbiol. 7. https://doi.org/10.3389/fmicb.2016.01642

Wickham, H., 2011. ggplot2. WIREs Comput. Stat. 3, 180–185. https://doi.org/10.1002/wics.147

Wilke, A., Harrison, T., Wilkening, J., Field, D., Glass, E.M., Kyrpides, N., Mavrommatis, K., Meyer, F., 2012. The M5nr: a novel non-redundant database containing protein sequences and annotations from multiple sources and associated tools. BMC Bioinformatics 13, 141. https://doi.org/10.1186/1471-2105-13-141

Wu, Y.-W., Simmons, B.A., Singer, S.W., 2016. MaxBin 2.0: an automated binning algorithm to recover genomes from multiple metagenomic datasets. Bioinformatics 32, 605–607. https://doi.org/10.1093/bioinformatics/btv638

Xie, W., Wang, F., Guo, L., Chen, Z., Sievert, S.M., Meng, J., Huang, G., Li, Y., Yan, Q., Wu, S., Wang, X., Chen, S., He, G., Xiao, X., Xu, A., 2011. Comparative metagenomics of microbial communities inhabiting deep-sea hydrothermal vent chimneys with contrasting chemistries. ISME J. 5, 414–426. https://doi.org/10.1038/ismej.2010.144

Zhang, J.-Z., Millero, F.J., 1993. The products from the oxidation of H2S in seawater. Geochim. Cosmochim. Acta 57, 1705–1718. https://doi.org/10.1016/0016-7037(93)90108-9

930
931 **Figures legends**

932
933
934 Figure 1. The sampling map with the location of Antarctic Peninsula (A) and Deception Island,
935 with Fumarole Bay and Whalers Bay geothermal sites highlighted (B). Distribution of collected
936 samples across environmental gradients at studied geothermal sites are described in C for Fumarole
937 Bay and D for Whalers Bay. *In situ* temperatures are represented in blue (glaciers) and orange
938 (fumaroles). The arrow indicates the direction of low and high values of temperature, salinity and
939 volcanic compounds, such as sulfate. Figure was retrieved from Bendia et al., 2018b.

940

941 Figure 2. Relative abundances of microbial community taxonomy based on annotation of reads
942 from shotgun metagenomics, represented at phylum (A) and class (B) levels. Environmental
943 temperatures and geothermal sites of each sample are represented. Taxonomy assignments were
944 performed based on best hit classifications and M5NR (non-redundant protein database), with an
945 e-value of $<1x10^{-5}$, minimum 50 bp alignment, and 60% identity. Co-occurrence network analysis
946 at the genus level are represented in (C), grouping triplicates of each sampling point and
947 highlighting the increases of environmental temperatures and complexity. Complexity was
948 calculated based on a set of measures, such as the number of nodes and edges, modularity, the
949 number of communities, average node connectivity, average path length, diameter, and cumulative
950 degree distribution.

951

952 Figure 3. Extended error plots for functional general profiles of microbial communities generated
953 through annotation of metagenomic reads, visualized through STAMP based on SEED
954 subsystems, are represented in (A). The *p* values were calculated using Fisher's exact two-sided
955 test and the confidence intervals were calculated by the method from Newcombe-Wilson.
956 Differences were considered significant at $p< 0.05$. PCA ordination was performed based on
957 functions at level 3 of the SEED subsystem (B). Heatmap is representing relative abundances of
958 level 1 functions (C). Samples are clustered and colored according to environmental temperature,
959 following the three different groups: 98 ^{o}C fumarole, <80 ^{o}C fumaroles and glaciers.

960

Figure 4. Extended error plots for functional profiles regarding metabolic pathways, including sulfur, nitrogen and carbon metabolisms, and stress response, including oxidative and osmotic, and heat/cold shock responses. Profiles were visualized through STAMP based on annotation of metagenomic reads using SEED subsystems. The *p* values are represented and were calculated using Fisher's exact two-sided test, with the confidence intervals calculated by the method from Newcombe-Wilson. Samples are clustered and colored according to environmental temperature, following the three different groups: 98 ºC fumaroles, <80 ºC fumaroles and glaciers.

Figure 5. Spearman correlation between taxonomic profile (A) (phylum level) and functional profile (level 1 SEED subsystem) (B) and environmental parameters. Only parameters that exhibited $p < 0.05$ in a correlation analysis are represented. The environmental parameters are: Temp (temperature), pH, EC (electrical conductivity), B, Cu, Fe, Zn, OM (organic matter), OC (organic carbon), P, Si, Na, K, Ca, Mg, sulfate, nitrogen, ammonia, nitrate, sand, silt, and clay.

Figure 6. Functional annotation of the 11 selected metagenome-assembled genomes (MAGs), including metabolic potential (A) and adaptive strategies (B). A black circle represents the presence of genes or complete gene cluster/pathway, and a yellow circle represents incomplete gene cluster or pathway. MAGs codes are represented on the upper side of figures, whereas their taxonomic classification based on GTDB-Tk and GhostKoala are at the bottom. Genes are presented here with identifiers of KEGG Orthology (KO), Clusters of Orthologous Groups (COG) or Enzyme Commission numbers (EC).

Table legends

Table 1. List of the 11 selected MAGs and their taxonomic classification based on GTDB-Tk and GhostKoala. Characteristics of total genome length, N50, GC content, redundancy and completeness (based on CheckM), and the genome quality status, are described.

992 **Supplementary Figures and Tables**

993

994 Figure S1. Relative abundances of microbial community taxonomy based on annotation of contigs,
995 represented at the phylum level. Contigs were constructed through IDBA-ud and annotated using
996 the Integrated Microbial Genomes & Microbiomes (IMG/M) system.

997

998 Figure S2. Extended error plots for functional profiles regarding DNA repair, helicase and
999 topoisomerase, protein biosynthesis, and transport and chemotaxis. Profiles were visualized
1000 through STAMP based on annotation of metagenomic reads using SEED subsystems. The *p* values
1001 are represented and were calculated using Fisher's exact two-sided test, with the confidence
1002 intervals calculated by the method from Newcombe-Wilson. Samples are clustered and colored
1003 according to environmental temperature, following the three different groups: 98 ^{o}C fumarole, <80
1004 ^{o}C fumaroles and glaciers.

1005

1006 Figure S3. A circular view of the 158 metagenome-assembled genomes (MAGs) that were
1007 recovered through anvi'o v. 5 pipeline and are represented with the mean coverage of contigs, and
1008 the MAGs redundancy, completeness, GC content, total reads mapped and number of SNVs
1009 reported. The clustering dendrogram in the center shows the hierarchical clustering of contigs
1010 based on their sequence composition, and their distribution across samples.

1011

1012 Figure S4. Heatmap representing the 13 high quality and 82 medium quality MAGs based on read
1013 mapping per sample with Z-score. Samples are clustered and colored according to environmental
1014 temperature, following the three different groups: 98 ^{o}C fumarole, <80 ^{o}C fumaroles and glaciers.

1015

1016

1017 Table S1. Physical-chemical parameters data per sample including temperature, pH, EC (electrical
1018 conductivity), B, Cu, Fe, Zn, OM (organic matter), OC (organic carbon), P, Si, Na, K, Ca, Mg,
1019 sulfate, nitrogen, ammonia, nitrate, sand, silt, and clay.

1020

1021 Table S2. General information about reads and contigs annotation.

1022

Table S3. *P*-values of Spearman correlations comparing taxonomic and functional profiles with the environmental data.

Table S4. A complete list of all reconstructed MAGs with their characteristics: taxonomic classification based on GTDB-Tk and GhostKoala, the total genome length, N50, GC content, redundancy and completeness, based on anvi'o and CheckM, and the genome quality status.

FIGURE 1

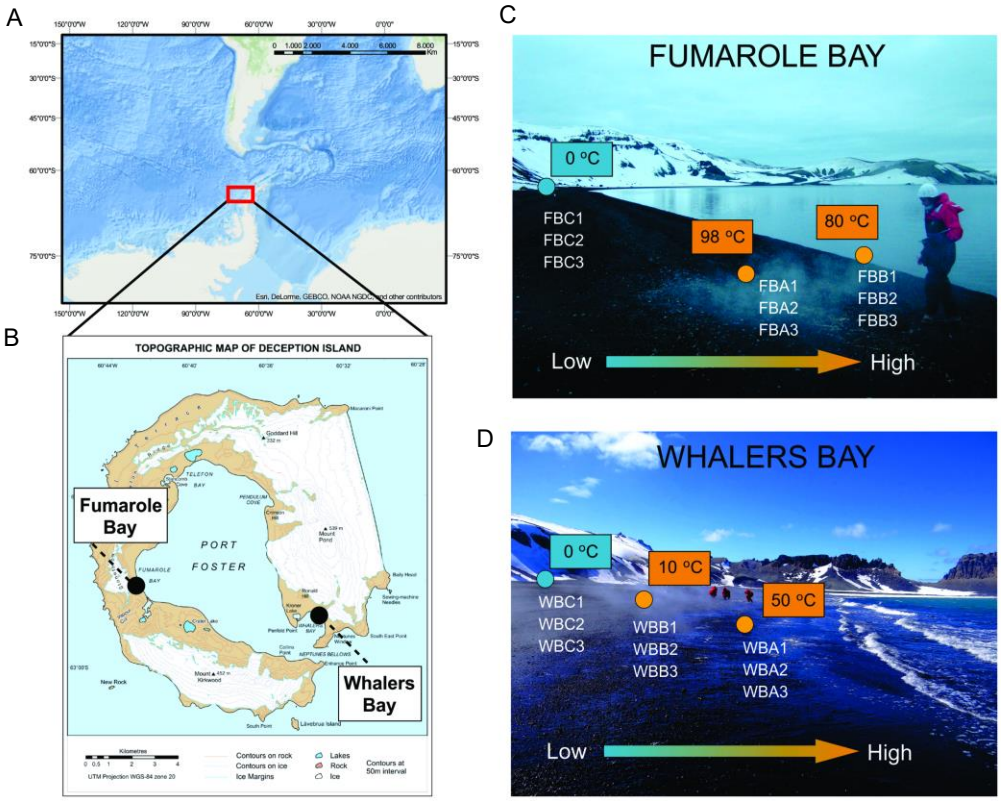

FIGURE 2

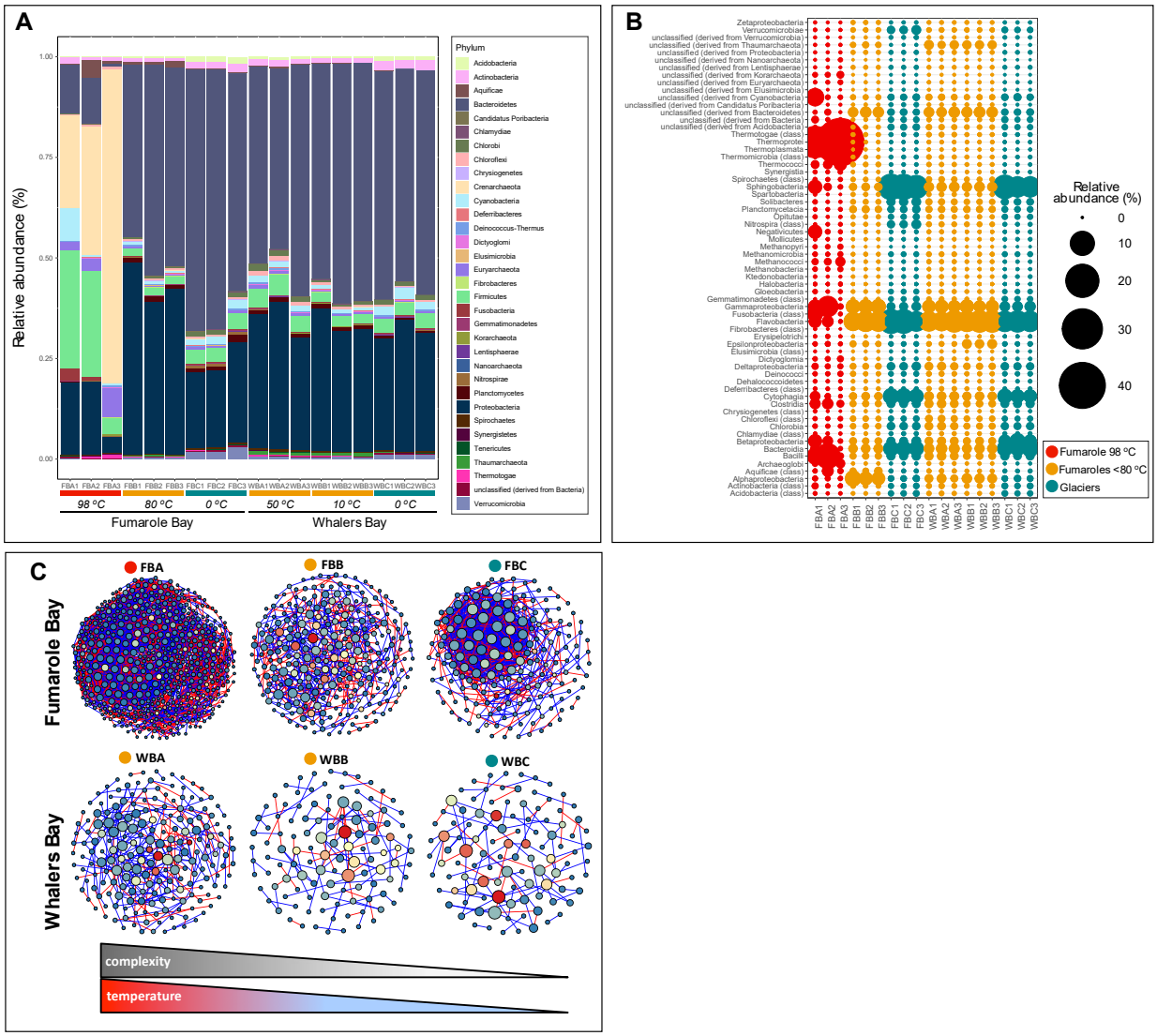

FIGURE 3

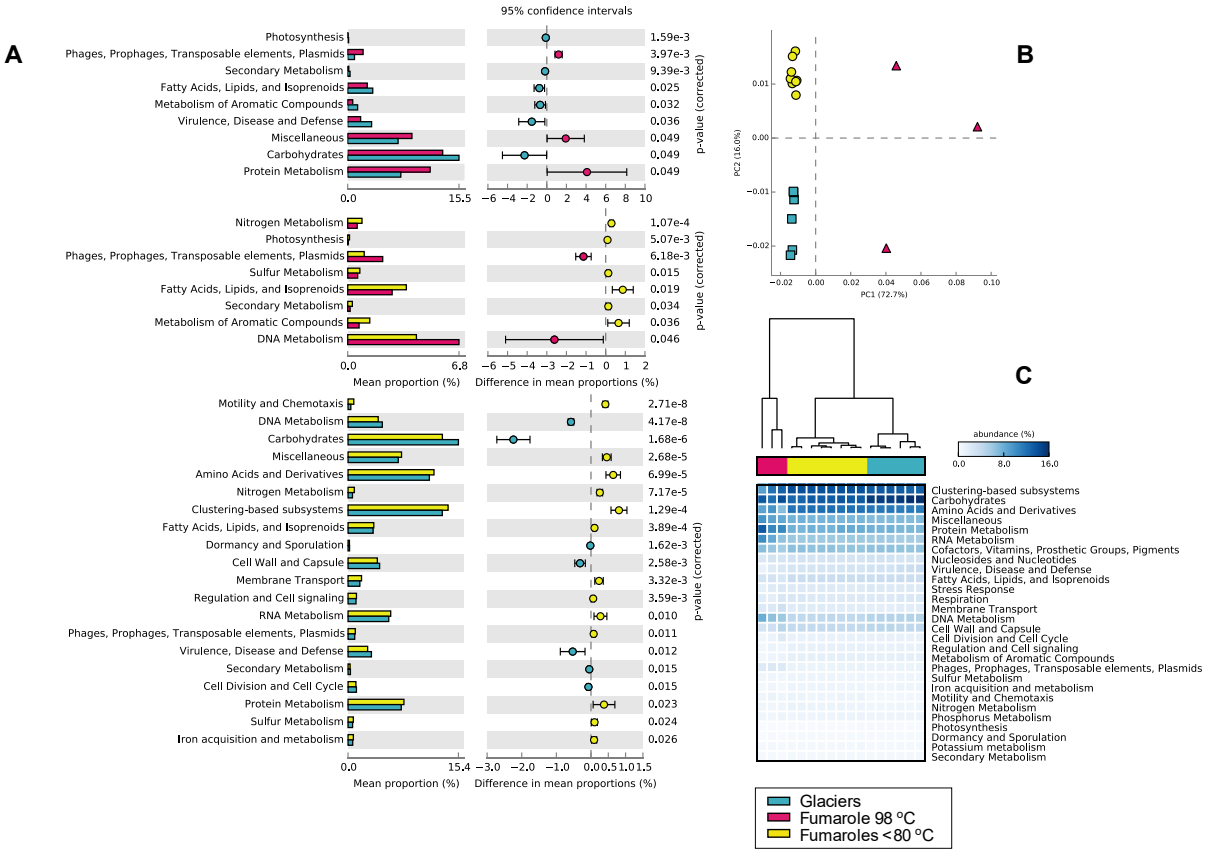

FIGURE 4

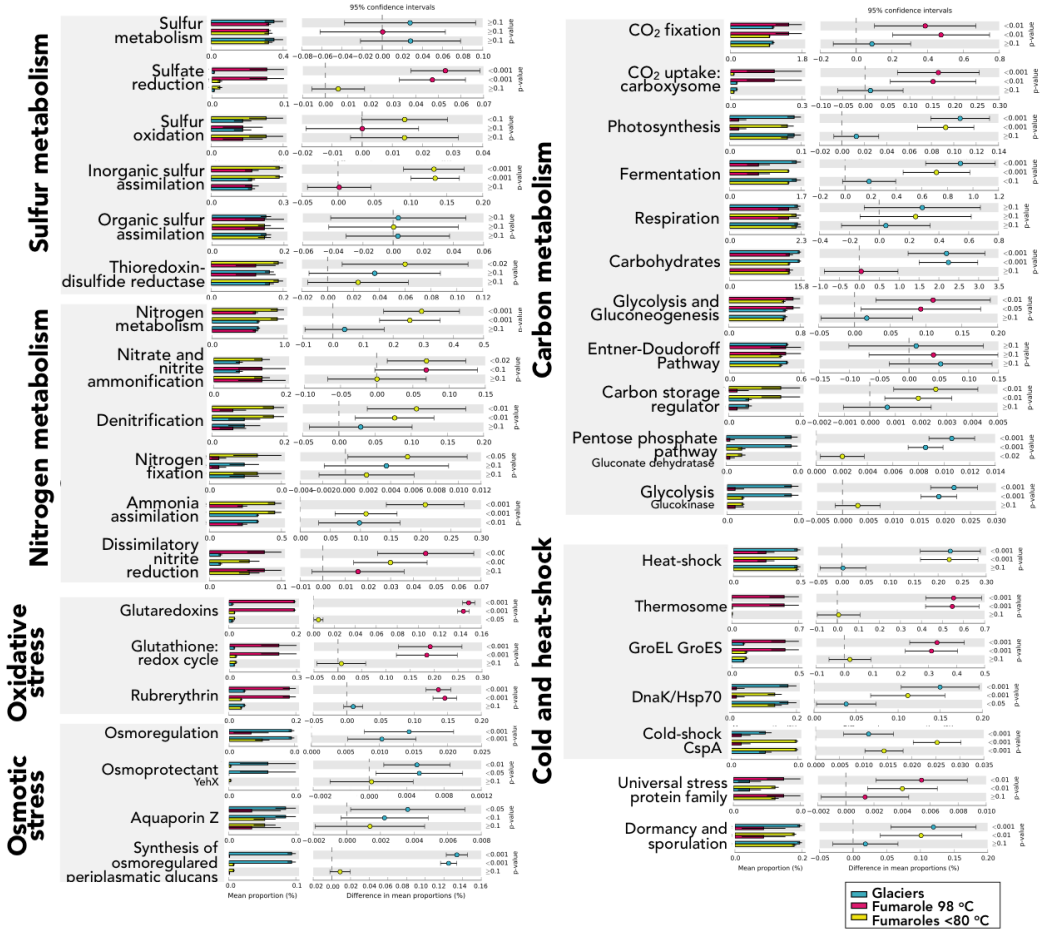

FIGURE 5

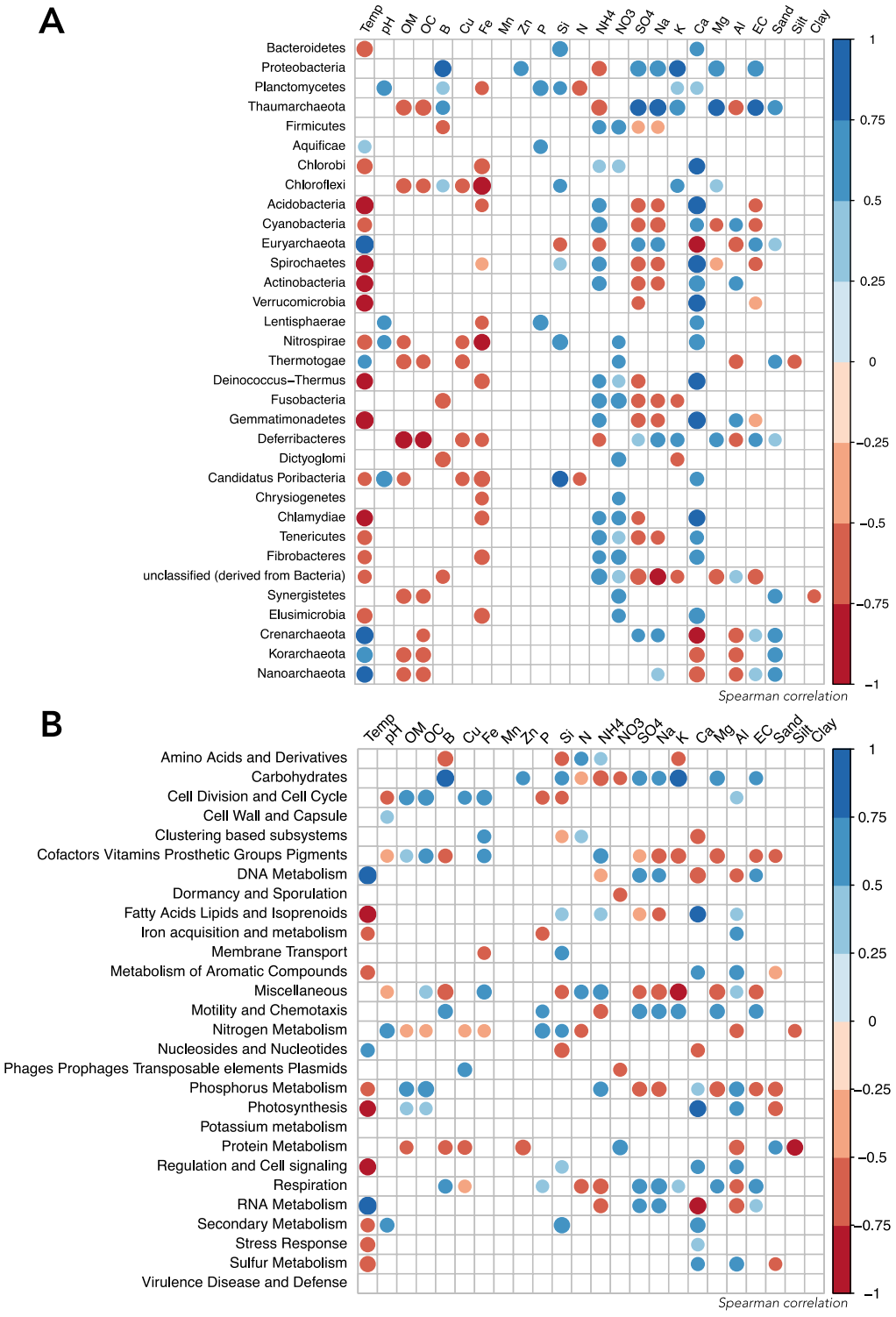

FIGURE 6

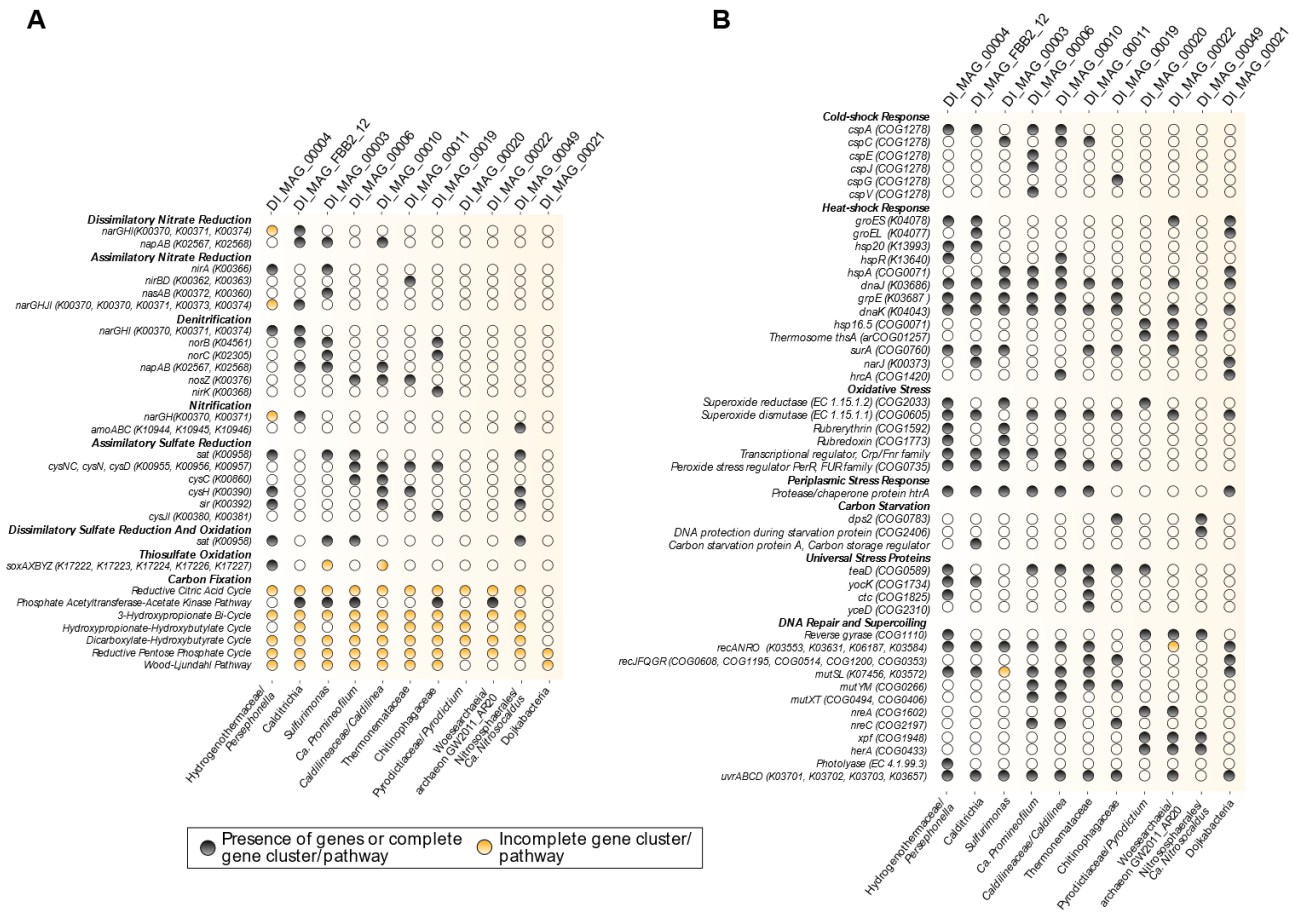

TABLE 1

MAG Code	KEGG/Ghost Koala taxonomy	GTDB-Tk taxonomy	Total Length	Contigs number	N50	GC content	Completeness	Redundancy	Draft Quality
DI_MAG_00003	*Sulfurimonas*	Bacteria; Campylobacterota; Campylobacteria; Campylobacterales; Thiovulaceae; *Sulfurimonas*	1,912,170	94	32,276	39.42	97.95	0.41	High
DI_MAG_00004	*Persephonella*	Bacteria; Aquificota; Aquificae; Hydrogenothermales; Hydrogenothermaceae	1,682,998	67	44,923	30.32	98.37	0.22	High
DI_MAG_00006	*Candidatus Promineofilum*	Bacteria; Chloroflexota; Anaerolineae; Promineofilales; Promineofilaceae	4,660,983	56	102,288	52.27	92.73	2.00	High
DI_MAG_00010	*Caldilinea*	Bacteria; Chloroflexota; Anaerolineae; Caldilineales; Caldilineaceae	4,473,267	92	90,197	57.82	96.36	0.91	High
DI_MAG_00011	Unknown	Bacteria; Bacteroidota; Bacteroidia; Cytophagales; Thermonemataceae	2,518,210	152	22,003	49.00	88.43	0.55	High
DI_MAG_00019	Unknown	Bacteria; Bacteroidota; Bacteroidia; Chitinophagales; Chitinophagaceae	3,082,789	324	10,795	37.53	62.85	7.88	Medium
DI_MAG_00020	*Pyrodictium*	Archaea; Crenarchaeota; Thermoprotei; Desulfurococcales; Pyrodictiaceae	1,071,537	28	68,816	47.76	75.27	0.47	Medium
DI_MAG_00021	Unknown	Bacteria; Patescibacteria; Dojkabacteria	734,971	8	176,471	31.53	77.27	1.72	Medium
DI_MAG_00022	archaeon GW2011_AR20	Archaea; Nanoarchaeota; Woesearchaeia	1,155,662	40	83,443	44.63	79.44	0.00	Medium
DI_MAG_00049	*Candidatus Nitrosocaldus*	Archaea; Crenarchaeota; Nitrososphaeria; Nitrososphaerales	982,006	145	6,877	32.09	60.52	1.94	Medium
DI_MAG_FBB2_12	*Caldithrix*	Bacteria; Calditrichota; Calditrichia	2,931,548	176	21,244	39.10	95.54	0.00	High